

InGaAs/AlInAs quantum cascade laser sources based on intra-cavity second harmonic generation emitting in 2.6-3.6 micron range

M.A. Belkin^{a*}, M. Jang^a, R.W. Adams^a, J. X. Chen^b, W. O. Charles^b, C. Gmachl^b, L. W. Cheng^c, F.-S. Choa^c, X. Wang^d, M. Troccoli^d, A. Vizbaras^e, M. Anders^e, C. Grasse^e, and M.-C. Amann^e

^aDepartment of Electrical and Computer Engineering, The University of Texas at Austin, Austin, TX 78758

^bDepartment of Electrical Engineering and MIRTHE, Princeton University, Princeton, NJ 08544

^cDepartment of Computer Science and Electrical Engineering, University of Maryland Baltimore County, Baltimore, MD 21250

^dAdtech Optics, Inc., 18007 Cortney Court, City of Industry, CA91748

^eWalter Schottky Institut, Technische Universität München, Garching 85748, Germany

*E-mail: mbelkin@ece.utexas.edu

ABSTRACT

We discuss the design and performance of quantum cascade laser sources based on intra-cavity second harmonic generation operating in at wavelengths shorter than 3.7 μm . A passive heterostructure tailored for giant optical nonlinearity is integrated on top of an active region and patterned for quasi-phases matching. We demonstrate operation of $\lambda \approx 3.6\mu\text{m}$, $\lambda \approx 3.0\mu\text{m}$, and $\lambda \approx 2.6\mu\text{m}$ devices based on lattice-matched and strain-compensated InGaAs/AlInAs/InP materials. Threshold current densities of typical devices with nonlinear sections are only 10-20% higher than that of the reference lasers without the nonlinear section. Our best devices have threshold current density of 2.2kA/cm² and provide approximately 35 μW of second-harmonic output at 2.95 μm at room temperature. The second-harmonic conversion efficiency is approximately 100 $\mu\text{W}/\text{W}^2$. Up to two orders of magnitude higher conversion efficiencies are expected in fully-optimized devices. **Keywords:** quantum cascade lasers, second harmonic generation, short wavelength, room temperature, intersubband, giant nonlinear susceptibility, quasi-phase matching

1. INTRODUCTION

InGaAs/AlInAs/InP quantum cascade lasers (QCL) have recently been developed into reliable high-power sources that operate continuous-wave (CW) at room-temperature (RT) in the spectral range 3.7-12 μm [1]. Their growth and fabrication process is compatible with telecommunication diode lasers production lines which makes manufacturing cost efficient. The spectral range 2.5-12 μm is called ‘molecular fingerprint region’; it contains a large number of molecular absorption lines and is highly important for chemical sensing. Widely-tunable QCL sources have been developed to address spectroscopic needs in this region. Examples include an external-cavity QCL tunable between 7.6 μm and 11.4 μm reported in Ref. [2] and a QCL source based on an array of distributed-feedback (DFB) devices with frequency output variable between 8 μm and 9.8 μm [3]. A 2.5-3.7 μm portion of the ‘molecular fingerprint region’ contains a number of absorption lines important for chemical sensing and spectroscopy. Ideally, one would want to have a device that can provide spectral coverage of the whole ‘molecular fingerprint region’. However, the operation of InGaAs/AlInAs/InP QCLs at 2.5-3.7 μm spectral range suffers from inter-valley scattering, even when highly strained heterostructures are used [4]. Diode lasers [5] and interband cascade lasers [6] can operate CW at $\lambda = 2.5\text{-}3.7\mu\text{m}$ but they cannot operate at RT at longer wavelengths. In addition, their growth and fabrication process is not compatible with that of telecommunication diode lasers. Heterostructures based on InAs/AlSb [7] and GaInAs/AlAsSb/InP [8] materials may be used to extend the operation of QCLs to the wavelengths shorter than 3.7 μm , but these devices are yet to demonstrate CW operation at RT and their fabrication is also not compatible with that of telecommunication diode lasers. We note that most spectroscopic application require a narrowband CW laser source with only about a milliwatt of output power.

Intra-cavity second-harmonic generation (SHG) has long been suggested as a mean to extend the spectral range of QCLs to shorter wavelengths [9-14]. However, none of these lasers operated at RT. Here we discuss an approach [15] for producing short-wavelength, high-performance QCL sources based on intra-cavity SHG. Our method allows extending the spectral range of RT CW InGaAs/AlInAs/InP QCLs to $\lambda=2.5\text{-}3.7\mu\text{m}$. We believe that these devices may provide a cost-effective solution for spectroscopic applications in the 2.5-3.7 μm range, and may lead to broadband QCL chips with spectral output tunable in the whole 2.5-10 μm spectral range and beyond (using both SHG light and fundamental light). We discuss the performance of our proof-of-principle QCLs operating at $\lambda=2.6, 3.0$ and $3.6\mu\text{m}$.

2. DEVICE DESIGN

The details of our devices design are shown in Fig. 1(a). Devices are grown on InP substrates using either lattice-matched or strain-compensated InGaAs/AlInAs heterostructures. A 400-600nm-thick nonlinear layer (NL) is grown epitaxial on top of a QCL active region. The NL contains multiple repetitions of a multi-quantum-well structure designed to have giant resonant optical nonlinearity associated with intersubband transitions [16]. A portion of the NL is then patterned into a ~50%-duty-cycle grating for quasi-phase-matching (QPM) [12,17] for SHG between TM_{00} modes. QPM allows us to generate SHG output in TM_{00} mode, which is important for practical applications. The separation of an active region and a NL allows us to optimize the two elements independently.

The NL is passive and increases optical losses in the laser cavity. However, the losses can be reduced to manageable values if we remove most of the NL to leave only a small section (200-400 μm long in the case of our devices) near the output facet as shown in Fig. 1(a). The upper waveguide cladding is then overgrown. We note that these processing steps are similar to those used for fabricating distributed feedback QCLs [18]. Devices are then processed into ridge-waveguide QCLs with 10-12 μm -wide ridges following standard procedure for.

To understand the expected device performance, we consider the laser structure designed for 3.6 μm SHG emission [15]. The laser is grown on an InP substrate, n-doped to $1\times 10^{17}\text{ cm}^{-3}$. First a 1.6- μm -thick active region, consisting 30 repetitions of a 2-phonon-resonance QCL structure [19], is grown; then a 400-nm-thick NL is grown on top of the active region. The NL consists of 24 repetitions of the structure depicted in Fig. 1(b). After NL patterning, the top waveguide cladding layers (3.5 μm of InP doped to $5\times 10^{16}\text{ cm}^{-3}$, followed by 0.5 μm of InP doped to $3\times 10^{18}\text{ cm}^{-3}$) are re-grown. Devices are processed into 10 μm -wide and 3mm-long ridge lasers. The intensity loss, (α_{NL}) and SHG nonlinearity ($\chi^{(2)}$) for TM-polarized light in the NL can be calculated using well-known expressions for intersubband absorption and optical nonlinearity [20]. Using the transition dipole moments shown in Fig. 1(b), the doping level in the NL, and assuming a typical transition linewidth of 20meV full width at half maximum (FWHM), we obtain $\alpha_{\text{NL}}(\omega)\approx 630\text{ cm}^{-1}$ and $\alpha_{\text{NL}}(2\omega)\approx 230\text{ cm}^{-1}$ for fundamental ($\lambda=7.2\mu\text{m}$) and SHG ($\lambda=3.6\mu\text{m}$) light, respectively, and $\chi^{(2)}=2.2\times 10^4\text{ pm/V}$. The loss

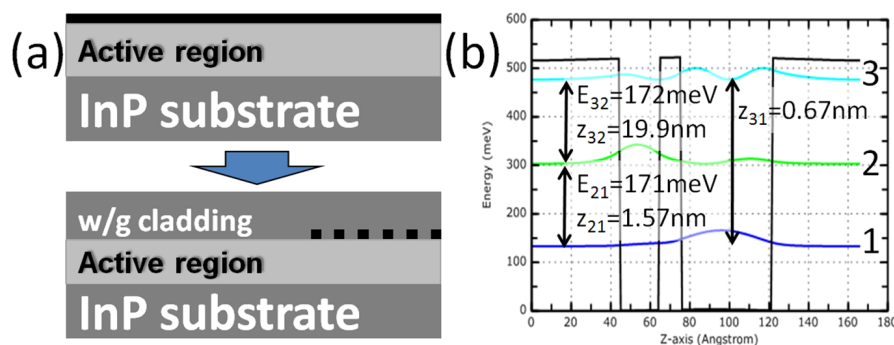


Fig. 1. (a) Schematic of the devices design and processing steps. Top panel shows a longitudinal cross section a QCL structure without top waveguide cladding. The nonlinear layer (shown in black) is positioned on top of the active region. The bottom panel shows a longitudinal cross section of the device with part of the nonlinear section removed, patterned for quasi-phase-matching of the SHG process, and then top waveguide cladding regrown. (b) Conduction band diagram of one period of a nonlinear structure for 7.2 μm to 3.6 μm frequency conversion. The layer sequence (in nm) is **9.0**/2.0/**1.1**/4.6 where AlInAs barriers are shown in bold and InGaAs wells are shown in regular font. The structure is lattice matched to InP. The center 3 nm of a 9 nm barrier is n-doped to $3\times 10^{17}\text{ cm}^{-3}$. Shown are energy levels, transition energies, and transition dipole moments.

for the TM_{00} mode in the waveguide with the nonlinear grating, $\alpha_{TM_{00GR}}$ is calculated to be $\alpha_{TM_{00GR}}(\omega)=40\text{cm}^{-1}$ and $\alpha_{TM_{00GR}}(2\omega)=13\text{cm}^{-1}$ for fundamental and SHG frequencies, respectively. TM_{00} modal loss at $\lambda=7.2\mu\text{m}$ in the laser waveguide without nonlinearity, $\alpha_{TM_{00LAS}}(\omega)$, is calculated to be 9.6cm^{-1} . The total round-trip distributed loss (α_{tot}) for a TM_{00} laser mode at $\lambda=7.2\mu\text{m}$ is then given as

$$\alpha_{\text{tot}}(\omega)=\alpha_m+(L_{GR}\alpha_{TM_{00GR}}(\omega)+L_{LAS}\alpha_{TM_{00LAS}}(\omega))/(L_{GR}+L_{LAS}), \quad (1)$$

where α_m is the mirror loss, L_{GR} is the length of the nonlinear grating section, and L_{LAS} is the length of the laser section without optical nonlinearity. For a TM_{00} mode in a 3mm-long device with $400\mu\text{m}$ nonlinear section we obtain $\alpha_m=4\text{cm}^{-1}$ and $\alpha_{\text{tot}}(\omega)=17.7\text{cm}^{-1}$. In comparison, the same calculation gives $\alpha_{\text{tot}}(\omega)=13.6\text{cm}^{-1}$ for a device of the same length without any nonlinearity. Thus, with proper design, the addition of the nonlinear section is only expected to increase the total loss in our devices by $\sim 30\%$.

The SHG power output is given as [9,17,21]

$$W(2\omega)=\frac{(2\omega)^2}{8\varepsilon_0c^3n(2\omega)n(\omega)n(\omega)}\left|\frac{\chi^{(2)}}{\pi}\right|^2\times\frac{(W(\omega))^2}{S_{\text{eff}}}\times l_{\text{eff}}^2, \quad (2)$$

where $W(\omega)$ is the pump power at the entrance of the nonlinear section, $W(2\omega)$ is the SHG power at the end of the nonlinear section, $n(\omega)$ is the refractive index at frequency ω , $|\chi^{(2)}/\pi|$ is the effective nonlinearity for the QPM process [17], and S_{eff} is the effective area of the beam's overlap with the nonlinear region [3,14]. We estimate S_{eff} to be approximately $5\times 10^3\mu\text{m}^2$ in our devices. The parameter l_{eff} is the effective nonlinear interaction length, which includes the effect of optical absorption of both fundamental and SHG waves, and is given as:

$$l_{\text{eff}}^2=\frac{e^{-\alpha_{2\omega}L_{GR}}\left(e^{-(\alpha_{\omega}-\alpha_{2\omega}/2)L_{GR}}-1\right)^2}{\left(\alpha_{\omega}-\alpha_{2\omega}/2\right)^2}, \quad (3)$$

where α_{ω} and $\alpha_{2\omega}$ are the net modal intensity losses for the fundamental and SHG waves in the section of the device with the nonlinear grating, and L_{GR} is the length of the nonlinear section. Equation 3 assumes a perfect first-order QPM [15] of the SHG process. We can estimate l_{eff} by taking $\alpha_{\omega}=\alpha_{TM_{00GR}}(\omega)-g_{TM_{00}}(\omega)=22\text{cm}^{-1}$, where $g_{TM_{00}}(\omega)=\alpha_{\text{tot}}(\omega)=17.7\text{cm}^{-1}$ (cf. Eq. (1)) is the modal gain, and $\alpha_{2\omega}=\alpha_{TM_{00GR}}(2\omega)=13\text{cm}^{-1}$. We then obtain $l_{\text{eff}}\approx 230\mu\text{m}$ for a nonlinear grating length $L=400\mu\text{m}$ and the SHG internal conversion efficiency $\eta_{\text{int}}\equiv W(2\omega)/(W(\omega))^2=2.3\text{mW}/\text{W}^2$ for 3mm-long devices with $400\mu\text{m}$ -long nonlinear sections. We may also define the 'external conversion efficiency' (η_{ext}) for the same device that links SHG power output through the front facet with fundamental power output through the front facet:

$$\eta_{\text{ext}}=\eta_{\text{int}}\frac{T_{2\omega}}{T_{\omega}^2e^{-2\alpha_{\omega}L_{GR}}}\approx 19\text{mW}/\text{W}^2, \quad (4)$$

where $T_{\omega}\approx T_{2\omega}\approx 0.7$ is power transmission through the front facet for fundamental and SHG light. Given typical Watt-level power output of modern QCLs [1], we may expect to generate several milliwatts of more of SHG output in our devices, when QPM and the nonlinear layer structure are fully optimized.

3. PROOF-OF-PRINCIPLE DEVICES PERFORMANCE

The results obtained with three of our proof-of-principle device designs are presented below. The power-current (L-I) characteristics for fundamental output for a $\lambda=3.6\mu\text{m}$ SHG device at room temperature and 80L are shown in Fig. 2(a). The laser was 3mm long, had a high reflectivity coating on the back facet, and had a $400\mu\text{m}$ -long nonlinear grating section (the longest available in our processing run) near the front facet. Also shown in Fig. 2(a) are the current-voltage (I-V) characteristic of the same device and the L-I curve for a 3mm-long reference laser without a nonlinear layer. Fig. 2(b) shows L-Is for SHG light for the best-performing 3mm-long devices with $400\mu\text{m}$ -long nonlinear section at room temperature and 80K. Fundamental power measurements were performed with a thermopile detector, SHG power measurements were performed with a calibrated InSb detector using optical filters to reject fundamental light. The data was corrected for an approximately 40% collection efficiency of our optical setup and the filters transmission. The data in Fig. 1(a) indicates that RT threshold current density for a reference laser was nearly identical to that of the device with a $400\mu\text{m}$ -long nonlinear section. This indicates that the nonlinear section adds less than 2cm^{-1} of optical loss to α_{tot} , cf. Eq. (4). This number is smaller than the 4cm^{-1} estimated theoretically, which is likely because the energy levels in the

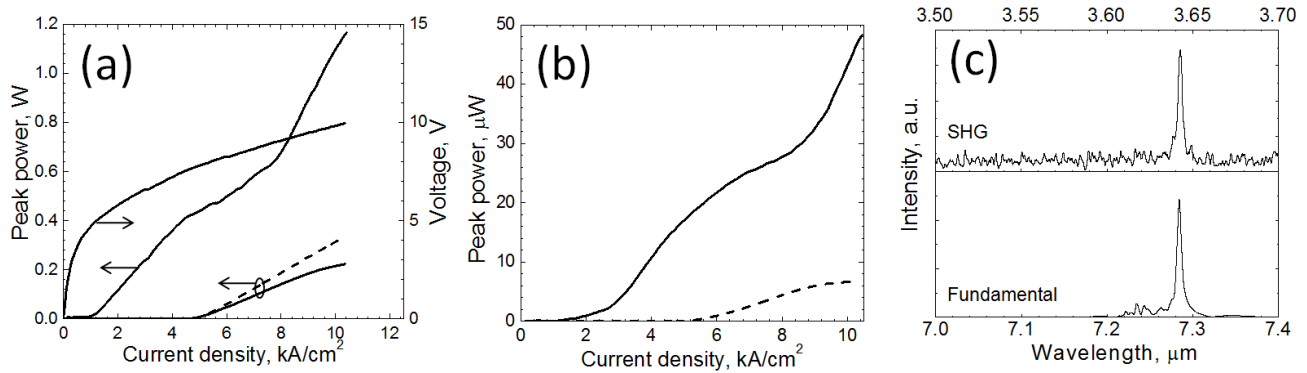


Fig. 2. (a) Current density-voltage characteristic at 298K and fundamental power-current density dependence at 298K (solid line, high threshold current density) and 80K (solid line, low threshold current density) of a 3mm-long device with a 400μm-long 31μm-period nonlinear grating. Also shown is the fundamental light output-current density characteristic of a 3mm-long reference device without the nonlinear section and with uncoated facets (dashed line). (b) SHG peak power output at 80K (solid line) and 298K (dashed line) as a function of current density for the device with a nonlinear grating in (a). (c) Room temperature emission spectra of the device in (b) at the peak SHG power output. Devices were operated with 50ns current pulses at a 50kHz repetition rate.

nonlinear section is not in exact resonance with the fundamental frequency. RT emission spectra for fundamental and SHG light of our devices are shown in Fig. 2(c). The spectra were taken using a Fourier-transform infrared spectrometer in rapid-scan mode. Using the fundamental power output of the devices without the nonlinear section we estimate the internal conversion efficiency of our device with the nonlinear section to be approximately 0.1W/W² at RT. This value is over a factor of 20 smaller than 2.3mW/W² estimated theoretically. This is most likely due to the fact that the energy levels in the NL are not fully resonant with fundamental and SHG transitions and thus the value of $\chi^{(2)}$ in the nonlinear section is significantly reduced. We note that if the actual energy position of level 3 is 30meV below the calculated value, the optical nonlinearity is reduced by a factor of 3.5 and the conversion efficiency is reduced by a factor of 12. Careful adjustment of the NL design for a given active region design is needed to produce devices with optimal SHG conversion efficiency.

SHG conversion efficiency is highly dependent on the QPM grating period in the NL. This is shown in Fig. 3, where we tested SHG conversion efficiencies of devices with QPM grating period in the range 24 μm to 37 μm. Devices with 31-μm-grating period displayed the highest SHG conversion efficiency. This is in close agreement with our theoretical estimates that predict the phase mismatch ($\Delta k=2k_{\omega_0}-k_{2\omega_0}$, where k_{ω_0} and $k_{2\omega_0}$ are the propagation constants for fundamental and SHG modes) between TM₀₀ modes of 2100 cm⁻¹ (The QPM grating period is then $\Lambda=2\pi/\Delta k\approx 30\mu\text{m}$ [17]).

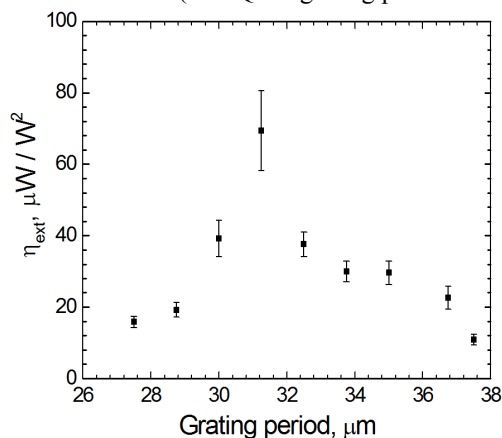


Fig. 3. (a) Dependence of η_{ext} on grating period for 3mm-long lasers with 170μm-long nonlinear section. For a given laser, the conversion efficiency varies as a function of pump current because of changes in the laser mode structure and emission wavelength. Plotted are the average values of η_{ext} for each laser with error bars indicating the range in which η_{ext} varies with current.

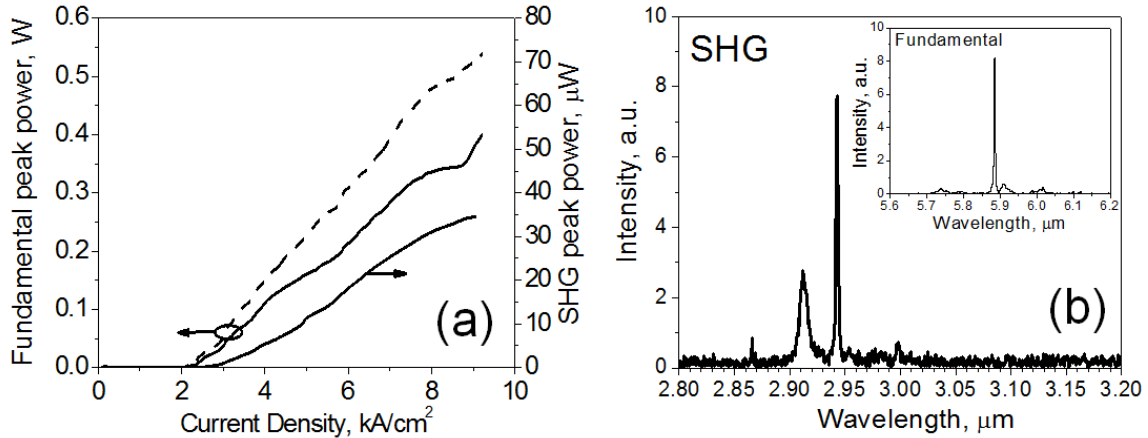


Fig. 4. (a) RT LI characteristics for fundamental output from a $\lambda \approx 2.95 \mu\text{m}$ SHG device with and without a nonlinear section (left axis, solid and dashed lines, respectively) and the LI characteristic for SHG power output (solid line, right axis). Devices were operated in pulsed mode with 100 kHz 50 ns pulses (b) Spectrum of RT SHG output from the device with the nonlinear section in (a). Inset: spectrum of the fundamental output from the same device.

Using $\sim 1\%$ strain-compensated InGaAs/AlInAs/InP heterostructures one could extend the spectral range of InGaAs/AlInAs SHG QCLs to wavelengths as short as $2.5 \mu\text{m}$. To demonstrate that, we present our results obtained with two proof-of-principle devices designed for SHG emission at $\lambda = 2.95 \mu\text{m}$ and $\lambda = 2.6 \mu\text{m}$.

Figure 4(a) shows the LI characteristics of fundamental and SHG emission from a device designed for SHG emission at $\lambda = 3.0 \mu\text{m}$. Also shown there is the LI characteristic of the device without the nonlinear section. The laser is based on an $\text{In}_{0.67}\text{Ga}_{0.33}\text{As}/\text{Al}_{0.57}\text{In}_{0.43}\text{As}$ heterostructure with $2.3\text{-}\mu\text{m}$ -thick active region and 460-nm -thick NL based on a bandstructure design similar to that shown in Fig. 1(b). The lasers were 3-mm -long with $400\text{-}\mu\text{m}$ -long nonlinear sections patterned for QPM. Devices operated at RT with threshold current density of 2.2kA/cm^2 and produced over $35 \mu\text{W}$ of SHG power output. Low threshold current density indicates that the lasers may be operated CW at RT when processed into buried heterostructures. RT emission spectra of a typical device are shown in Fig. 4(b). Threshold current density of devices with the nonlinear section was similar to that of devices without the nonlinear section although threshold current density increase of $\sim 30\%$ was expected for devices with the nonlinear section. Similarly to the $\lambda = 3.6 \mu\text{m}$ devices discussed above, this indicates that additional adjustment of the NL structure may be needed to make $\chi^{(2)}$ fully resonant for the SHG process. More details of the device design and performance will be presented elsewhere [22].

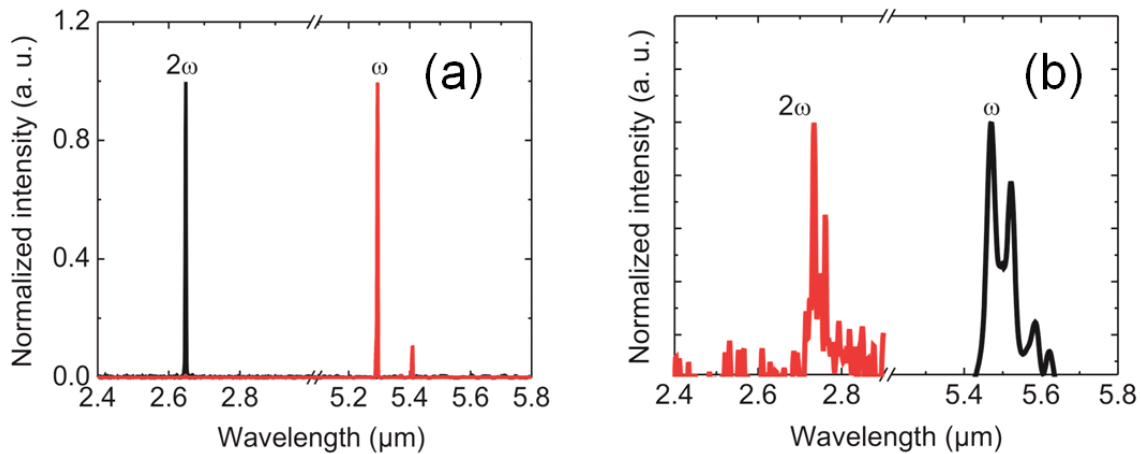


Fig. 5. (a) Spectra of fundamental (ω) and SHG (2ω) output from a $\lambda \approx 2.6 \mu\text{m}$ SHG QCL at 80K . (b) Spectra of fundamental (ω) and SHG (2ω) output from a $\lambda \approx 2.6 \mu\text{m}$ SHG QCL at RT.

Figure 5 shows the emission spectra of a $\lambda=2.6\mu\text{m}$ SHG QCL with NL based on $\text{In}_{0.65}\text{Ga}_{0.35}\text{As}/\text{Al}_{0.55}\text{In}_{0.45}\text{As}$ heterostructure. The laser provided over 1mW of SHG output at 80K and approximately 10 μW of SHG output at RT. The laser consisted of an approximately 1.5- μm -thick active region and an approximately 800-nm-thick nonlinear layer based on a bandstructure design similar to that shown in Fig. 1(b). Details of the device design and performance will be presented elsewhere [23].

4. CONCLUSION AND OUTLOOK

In conclusion, we discussed a new design architecture for short-wavelength InGaAs/AlInAs QCL sources based on intracavity SHG and demonstrated a operation of proof-of-principle devices with emission wavelengths in the range 2.6-3.6 μm . Our best devices provide over 35 μW of SHG output at $\lambda\approx 2.95\mu\text{m}$ at RT with threshold current density of only 2.2kA/cm². Our theoretical and experimental results indicate that RT CW operation of the proposed SHG QCLs is possible with proper device thermal packaging. The SHG power output of these devices is expected to improve to provide conversions efficiency of over 2mW/W². Given multi-Watt-level power output of current state-of-the-art QCLs, SHG QCLs presented in this work may produce over 10s of mW of output in the spectral range 2.5-3.7 μm , when fully optimized.

ACKNOWLEDGEMENTS

The University of Texas group acknowledges financial support from the Texas Higher Education Coordinating Board ‘Norman Hackerman Advanced Research Program’ award. Princeton University and the University of Maryland, Baltimore County teams acknowledge financial support from the NSF MIRTHE center. Walter Schottky Institut group acknowledges the financial support from the excellence cluster ‘Nano Initiative Munich (NIM)’.

REFERENCES

- [1] See, e.g., M. Razeghi, ‘‘High-performance InP-based mid-IR quantum cascade lasers,’’ *IEEE J. Sel. Top. Quant. Electron.* **15**, 941 (2009); N. Bandyopadhyay, Y. Bai, B. Gokden, A. Myzaferi, S. Tsao, S. Slivken, and M. Razeghi, ‘‘Watt level performance of quantum cascade lasers in room temperature continuous wave operation at $\lambda\sim 3.76\mu\text{m}$,’’ *Appl. Phys. Lett.* **97**, 131117 (2010); S. Slivken, A. Evans, W. Zhang, and M. Razeghi, ‘‘High-power, continuous-wave operation intersubband laser for wavelengths greater than 10 μm ,’’ *Appl. Phys. Lett.* **90**, 151115 (2007).
- [2] A. Hugi, R. Terazzi, Y. Bonetti, A. Wittmann, M. Fischer, M. Beck, J. Faist and E. Gini, ‘‘External cavity quantum cascade laser tunable from 7.6 to 11.4 μm ,’’ *Appl. Phys. Lett.* **95**, 061103 (2009).
- [3] B.G. Lee, H.A. Zhang, C. Pflügl, L. Diehl, M.A. Belkin, M. Fischer, A. Wittmann, J. Faist, F. Capasso, ‘‘Broadband distributed-feedback quantum cascade laser array operating from 8.0 to 9.8 μm ,’’ *IEEE Photon. Technol. Lett.* **21**, 914 (2009).
- [4] See, e.g., W.T. Masselink, M.P. Semtsiv, S. Dressler, M. Ziegler, M. Wienold, ‘‘Physics, growth, and performance of (In,Ga)As-AlP/InP quantum-cascade lasers emitting at $\lambda<4\mu\text{m}$,’’ *Phys. Stat. Sol. (b)* **244**, 2906 (2007).
- [5] See, e.g., L. Shterengas, G. Belenky, T. Hosoda, G. Kipshidze, and S. Suchalkin, ‘‘Continuous wave operation of diode lasers at 3.36 μm at 12 $^{\circ}\text{C}$,’’ *Appl. Phys. Lett.* **93**, 011103 (2008).
- [6] See, e.g., C.L. Canedy, W.W. Bewley, J.R. Lindle, J.A. Nolde, D.C. Larrabee, C.S. Kim, M. Kim, I. Vurgaftman, and J.R. Meyer, ‘‘Interband Cascade Lasers with Wavelengths Spanning 2.9 μm to 5.2 μm ,’’ *J. Electron. Mat.* **37**, 1780 (2008).
- [7] See, e.g., J. Devenson, O. Cathabard, R. Teissier, and A. N. Baranov, ‘‘High temperature operation of $\lambda\approx 3.3\mu\text{m}$ quantum cascade lasers,’’ *Appl. Phys. Lett.* **91**, 141106 (2007).
- [8] See, e.g., S.Y. Zhang, D. G. Revin, J. W. Cockburn, K. Kennedy, A. B. Krysa, and M. Hopkinson, ‘‘ $\lambda\sim 3.1\mu\text{m}$ room temperature InGaAs/AlAsSb quantum cascade lasers,’’ *Appl. Phys. Lett.* **94**, 031106 (2009).
- [9] C. Gmachl, A. Belyanin, D.L. Sivco, M.L. Peabody, N. Owschimikow, A.M. Sergent, F. Capasso, ‘‘Optimized second harmonic generation in quantum cascade lasers,’’ *IEEE J. Quantum Electron.* **39**, 1345 (2003).
- [10] O. Malis, A. Belyanin, D.L. Sivco, J. Chen, A.M. Sergent, C. Gmachl, A.Y. Cho, ‘‘Milliwatt second-harmonic generation in QC lasers with modal phase-matching,’’ *Electron. Lett.* **40**, 1586 (2004).
- [11] J.-Y. Bengloan, A. De Rossi, V. Ortiz, X. Marcadet, M. Calligaro, I. Maurin, and C. Sirtori, ‘‘Intracavity sum-frequency generation in GaAs quantum cascade lasers,’’ *Appl. Phys. Lett.* **84**, 2019 (2004).

- [12] M.A. Belkin, M. Troccoli, L. Diehl, F. Capasso, A.A. Belyanin, D.L. Sivco, A.Y. Cho, "Quasi-phase matching of second-harmonic generation in quantum cascade lasers by Stark shift of electronic resonances," *Appl. Phys. Lett.* **88**, 201108 (2006).
- [13] M. Austerer, C. Pflugl, S. Golka, W. Schrenk, A.M. Andrews, T. Roch, and G. Strasser, "Coherent 5.35 μm surface emission from a GaAs-based distributed feedback quantum cascade laser," *Appl. Phys. Lett.* **88**, 121104 (2006)
- [14] M. Giovannini, M. Beck, N. Hoyler, and J. Faist, "Second harmonic generation in (111)-oriented InP-based quantum cascade laser," *J. Appl. Phys.* **101**, 103107 (2007).
- [15] M. Jang, R.W. Adams, J.X. Chen, W.O. Charles, C. Gmachl, L.W. Cheng, F.-S. Choa, and M.A. Belkin, "Room-temperature operation of 3.6 μm InGaAs/AlInAs quantum cascade laser sources based on intracavity second harmonic generation," *Appl. Phys. Lett.* **97**, 141103 (2010).
- [16] See, e.g., C. Sirtori, F. Capasso, D.L. Sivco, S.N.G. Chu, and A.Y. Cho, "Observation of large second-order susceptibility via intersubband transitions at $\lambda \sim 10\mu\text{m}$ in asymmetric coupled AlInAs/GaInAs quantum wells," *Appl. Phys. Lett.* **59**, 2302 (1991).
- [17] Boyd, R. W. *Nonlinear Optics* (3rd ed., Academic Press, New York, 2008).
- [18] See, e.g., S. Blaser, D.A. Yarekha, L. Hvozdar, Y. Bonetti, A. Muller, M. Giovannini, and J. Faist, "Room-temperature, continuous-wave, single-mode quantum-cascade lasers at $\lambda \approx 5.4\mu\text{m}$," *Appl. Phys. Lett.* **86**, 041109 (2005).
- [19] M. Beck, D. Hofstetter, T. Aellen, J. Faist, U. Oesterle, M. Illegems, E. Gini, H. Melchior, "Continuous Wave Operation of a Mid-Infrared Semiconductor Laser at Room Temperature," *Science* **295**, 301 (2002).
- [20] See, e.g., *Intersubband Transitions in Quantum Wells II*, H.C. Liu and F. Capasso, eds., Semiconductors and Semimetals Vol. 66 (Academic Press, San Diego, CA).
- [21] M. A. Belkin, F. Capasso, A. Belyanin, D. L. Sivco, A. Y. Cho, D. C. Oakley, C. J. Vineis, and G. W. Turner., "Terahertz quantum-cascade-laser source based on intracavity difference-frequency generation," *Nature Photonics* **1**, 288-292 (2007) and supplementary information to the paper.
- [22] M. Jang, X. Wang, M. Troccoli, and M.A. Belkin, "Room-temperature operation of $\lambda \approx 2.95\mu\text{m}$ In_{0.67}Ga_{0.33}As/Al_{0.57}In_{0.43}As quantum cascade laser source based on intra-cavity second harmonic generation," manuscript in preparation.
- [23] A. Vizbaras, M. Anders, S. Katz, C. Grasse, G. Boehm, R. Meyer, M.A. Belkin, and M.-C. Amann, "Room-temperature $\lambda \approx 2.6\mu\text{m}$ quantum cascade laser sources based on intracavity second-harmonic generation," under review.